MICROCOPY RESOLUTION TEST CHART

NATIONAL BUREAU OF STANDARDS-1963-A

NSWC TR 85-402

DISPERSION CHARACTERISTICS OF A HELIX LOADED WAVEGUIDE

BY H. CROSBY J. CHOE A. KRALL

RESEARCH AND TECHNOLOGY DEPARTMENT

1 SEPTEMBER 1985

DTIC
SELECTE
APR 0 8 1986
S
D

NAVAL SURFACE WEAPONS CENTER

Dahlgren, Virginia 22448-5000 ● Silver Spring, Maryland 20903-5000

86 4 7 12 5

SECURITY CLASSIFICATION OF THIS PAGE *(When Data Entered)*

REPORT DOCUMENTATION PAGE		READ INSTRUCTIONS BEFORE COMPLETING FORM
1. REPORT NUMBER NSWC TR 85-402	**2. GOVT ACCESSION NO.** *ADA 166 444*	**3. RECIPIENT'S CATALOG NUMBER**
4. TITLE (and Subtitle) DISPERSION CHARACTERISTICS OF A HELIX LOADED WAVEGUIDE		**5. TYPE OF REPORT & PERIOD COVERED** FY 85
		6. PERFORMING ORG. REPORT NUMBER
7. AUTHOR(s) H. Crosby J. Choe A. Krall		**8. CONTRACT OR GRANT NUMBER(s)**
9. PERFORMING ORGANIZATION NAME AND ADDRESS Naval Surface Weapons Center (Code R43) 10901 New Hampshire Ave. Silver Spring, MD 20903-5000		**10. PROGRAM ELEMENT, PROJECT, TASK AREA & WORK UNIT NUMBERS**
11. CONTROLLING OFFICE NAME AND ADDRESS		**12. REPORT DATE**
		13. NUMBER OF PAGES 42
14. MONITORING AGENCY NAME & ADDRESS(if different from Controlling Office)		**15. SECURITY CLASS. (of this report)** UNCLASSIFIED
		15a. DECLASSIFICATION/DOWNGRADING SCHEDULE

16. DISTRIBUTION STATEMENT (of this Report)

Approved for public release; distribution is unlimited.

17. DISTRIBUTION STATEMENT (of the abstract entered in Block 20, if different from Report)

18. SUPPLEMENTARY NOTES

19. KEY WORDS (Continue on reverse side if necessary and identify by block number)

Helix Loaded Waveguide
Resonant Cavity
Dispersion Curves
Mode Identification

20. ABSTRACT (Continue on reverse side if necessary and identify by block number)

The dispersion characteristics of a helix loaded waveguide have been experimentally investigated. Helix loaded waveguides are of interest as a slow wave structure that can be employed to increase the bandwidth of gyroton amplifiers. The structure consists of helical wires contained concentrially in a cylindrical conductor. The helical wires are close enough together to form a helical sheath justifying the assumption of azimuthal symmetry. The relevant physical parameters are the pitch angle (ϕ) and the ratio of the

DD FORM 1473 EDITION OF 1 NOV 65 IS OBSOLETE
1 JAN 73
S/N 0102-LF-014-6601

20. (Cont.)

helix radius (R_h) to the conductor radius (R_c). The dispersion relations for the general azimuthal mode number are obtained for both the fast hybrid and the helix modes.

FOREWORD

The dispersion characteristics of. helix loaded waveguides have been experimentally investigated. Helix loaded waveguides are of interest as a slow wave structure that can be employed to increase the bandwidth of gyroton amplifiers. The structure consists of helical wires contained concentrially in a cylindrical conductor. The helical wires are close enough together to form a helical sheath justifying the assumption of azimuthal symmetry. The relevant physical parameters are the helix pitch angle (ϕ) and the ratio of the helix radius (R_h) to the conductor radius (R_c). The dispersion relations for the general azimuthal mode number are obtained for both the fast hybrid and the helix modes.

Approved by:

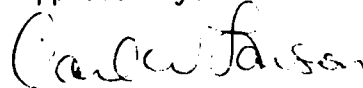CARL W. LARSON, Head
Radiation Division

Accesion For		
NTIS CRA&I		☑
DTIC TAB		☐
Unannounced		☐
Justification		
By		
Distribution /		
Availability Codes		
Dist	Avail and / or Special	
A-1		

CONTENTS

ILLUSTRATIONS

SECTION 1

INTRODUCTION

The gyrotron is a vacuum tube capable of producing high (10 kW avg) power output in the millimeter and sub-millimeter wavelength region. Its recent application to millimeter wave radar and nuclear fusion could be greatly enhanced if wide instantaneous bandwidths were available. The theoretical papers of Choe and Uhm[1,2] indicate that wide instantaneous bandwidths are possible with various slow wave structures. The purpose of this project is to investigate various slow wave structures to experimentally verify the new theory so that it can be used in the development of the gyrotron.

In a microwave tube such as a gyrotron the energy in an electron beam is converted to RF energy. Figure 1 shows a dispersion curve for an electron beam mode $\omega_B(k)$, and a dispersion curve for the vacuum waveguide mode, $\omega_G(k)$. The dispersion curve for the electron beam is given by

$$\omega_B = kv_z + \omega_c$$

$$\omega_c = \frac{eB_0}{mc}$$

where v_z is the velocity of the electron in the axial direction, ω_c is the cyclotron frequency, e the charge on an electron, B_0 the D.C. magnetic field strength, m the electron mass, c the speed of light in a vacuum, and k is the

axial wavenumber. The dispersion curve for the vacuum waveguide is dependent on the internal slow wave structure. Gain occurs only where the two dispersion curves ω_B and ω_G intersect. For the tube to be broadband the shape of the ω_G curve can be altered so that $\omega_G \approx \omega_B$ over a broad range of frequencies. The reason ω_G, not ω_B, is changed is that it is much easier to change a slow wave structure in a waveguide than the electron gun characteristcs or the magnetic field structures that control the electron trajectory.

One purpose of these experiments is to investigate how the parameters of a slow wave structure affect the shape of the dispersion curve, ω_G. Specifically, in this experiment the dispersion characteristics of a sheath helix loaded waveguide are investigated. A sheath helix is a structure composed of many parallel wire helices. As the wire thickness and the spacing between the wires approach zero, the resulting structure is an electrically smooth sheath. The conductivity of the sheath is infinite in the direction of the helices and zero perpendicular to this direction. Figure 2 is a photograph of an experimental helix. The thin closely spaced wires make it a good approximation to a sheath helix. A diagram of this structure is shown in Figure 3. The parameters that can be varied to alter the dispersion curve are the helix pitch angle, ϕ, and the ratio, R_h/R_c, of the helix radius to the radius of the conducting cylinder.

The resonant frequencies of a sheath helix loaded cavity were measured experimentally. From a large number of possible resonances a particular family of resonances, belonging to a family of transverse electric modes commonly used in gyrotrons, were identified. Positive identification of the modes was based on determining the azimuthal and axial mode numbers. By

counting the number of nulls in the output energy of the cavity as a metal probe was pulled along or rotated about the axis of the cavity, the axial and azimuthal mode numbers were determined respectively; the number of nulls being the mode number. Once the family of resonances had been identified, the dispersion characteristic was obtained by plotting the resonant frequency of each family member against its corresponding axial cavity wavelength.

SECTION 2

THEORY

As illustrated in Figure 3, the system configuration consists of a helix of radius R_h located inside and concentric with a cylindrical conducting waveguide of radius R_c. Cylindrical polar coordinates (r, θ, z) are introduced in the present analysis. In computing the properties of a helix, we assume that conducting wires in the helix are very thin and close together thereby replacing the helix by a helically conducting cylindrical sheet of radius R_h. This sheet is perfectly conducting in the helix direction making an angle ϕ, the pitch angle, with a plane normal to the axis of the system. The unit vector $\hat{e}_\phi$ of the helical wires is given by

$$\hat{e}_\phi = \cos \phi \, \hat{e}_\theta + \sin \phi \, \hat{e}_z, \tag{1}$$

where $\hat{e}_\theta$ and $\hat{e}_z$ are the unit vecters along the aximuthal and axial directions, respectively.

In the subsequent analysis, we adopt a normal mode approach in which all components of the electromagnetic field are assumed to vary according to

$$\psi(\underset{\sim}{x}, t) = \psi(r) \exp\{i(\ell\theta + kz - \omega t)\}, \tag{2}$$

where ω is the eigenfrequency, k is the axial wave number, and ℓ is the azimuthal harmonic number. The Maxwell equations for the electric and

magnetic field amplitudes can be expressed as

$$\nabla X \underset{\sim}{E}(\underset{\sim}{x}) = i(\omega/c)\underset{\sim}{B}(\underset{\sim}{x}),$$
$$\nabla X \underset{\sim}{B}(\underset{\sim}{x}) = (4\pi/c)\underset{\sim}{J}(\underset{\sim}{x}) - i(\omega/c)\underset{\sim}{E}(\underset{\sim}{x}) \tag{3}$$

where $\underset{\sim}{E}(\underset{\sim}{x})$ and $\underset{\sim}{B}(\underset{\sim}{x})$ are the electric and magnetic fields, and $\underset{\sim}{J}(\underset{\sim}{x})$ is the electric current density, which vanishes except at $r=R_h$.

Three boundary conditions must be satisfied at the helix of radius R_h. The tangential component of the electric field at surface of the helix must be perpendicular to the helix direction, i.e.,

$$E_z^i \sin \phi + E_\theta^i \cos \phi = 0 \tag{4}$$

$$E_z^0 \sin \phi + E_\theta^0 \cos \phi = 0. \tag{5}$$

The tangential component of electric field must be continuous across the helix, i.e.,

$$E_z^i = E_z^0, \quad E_\theta^i = E_\theta^0 . \tag{6}$$

The tangential component of magnetic field parallel to the helix direction must be continuous across the helix, i.e.,

$$B_z^i \sin \phi + B_\theta^i \cos \phi = B_z^0 \sin \phi + B_\theta^0 \cos \phi, \tag{7}$$

since there can be no current in the surface perpendicular to this direction. In Equations (4)-(7), the superscripts i and 0 represent $\psi^i = \lim_{\delta \to 0_+} \psi(R_h - \delta)$ and $\psi^0 = \lim_{\delta \to 0_+} \psi(R_h + \delta)$, respectively, at the helix boundary $r = R_h$.

Making use of Equation (3), it is straightforward to show that the differential equation for the axial components of the electric and magnetic fields is given by

$$\left(\frac{1}{r}\frac{\partial}{\partial r} r \frac{\partial}{\partial r} - \frac{\ell^2}{r^2} + \frac{\omega^2}{c^2} - k^2\right)\left\{\begin{array}{c} E_z(r) \\ B_z(r) \end{array}\right\} = 0, \tag{8}$$

except at $r = R_h$.

The solution to Equation (8) is

$$E_z(r) = a\left\{\begin{array}{l} J_\ell(pr), \quad 0 < r < R_h \\ J_\ell(\eta) \dfrac{N_\ell(\xi)J_\ell(pr) - J_\ell(\xi)N_\ell(pr)}{J_\ell(\eta)N_\ell(\xi) - J_\ell(\xi)N_\ell(\eta)}, \quad R_h < r < R_c, \end{array}\right. \tag{9}$$

for the electric field and

$$B_z(r) = b\left\{\begin{array}{l} J_\ell(pr), \quad 0 < r < R_h \\ J_\ell'(\eta) \dfrac{N_\ell'(\xi)J_\ell(pr) - J_\ell'(\xi)N_\ell(pr)}{J_\ell'(\eta)N_\ell'(\xi) - J_\ell'(\xi)N_\ell'(\eta)}, \quad R_h < r < R_c, \end{array}\right. \tag{10}$$

for the magnetic field. In Equations (9) and (10), a and b are constants, $J_\ell(x)$ and $N_\ell(x)$ are the Bessel functions of order ℓ of the first and second

kinds, respectively. The prime (') denotes $(d/dx)J_\ell(x)$ and $(d/dx)N_\ell(x)$, and the parameters η and ξ are defined by

$$\eta^2 = \xi^2 R_h^2/R_c^2 = p^2 R_h^2 = (\omega^2/c^2 - K^2)R_h^2 \tag{11}$$

From the Equation (3) and the skew boundary conditions in Equations (4)-(6), we can show the relationship of the coefficients is

$$\frac{b}{a} = i\frac{cp}{\omega} \frac{J_\ell(\eta)}{J'_\ell(\eta)}\left(\frac{k\ell}{p^2 R_h} - \tan \phi\right). \tag{12}$$

The azimuthal component of the magnetic field $B_\theta(r)$ is expressed as

$$B_\theta(r) = i\frac{\omega}{cp^2} \frac{\partial}{\partial r} E_z(r) - \frac{k\ell}{rp^2} B_z(r) \tag{13}$$

from Equation (3). The dispersion relation of the electromagnetic wave in a helix-loaded waveguide is obtained by substitution of Equations (10) and (13) into Equation (7), and by making use of Equation (12). After tedious but straightforward algebra, we obtain the resultant dispersion relation

$$D(\omega,k,\phi) = \frac{\omega^2}{c^2} - \frac{f(\xi,\eta)}{R_c^2}\left(\tan \phi - \frac{k\ell}{p^2 R_h}\right)^2 = 0, \tag{14}$$

where the function $f(\xi,\eta)$ is defined by

$$f(\xi,\eta) = -\xi^2 \frac{J_\ell(\eta)J_\ell'(\xi)}{J_\ell(\xi)K_\ell'(\eta)} \frac{J_\ell(\xi)N_\ell(\eta) - J_\ell(\eta)N_\ell(\xi)}{J_\ell'(\xi)N_\ell'(\eta) - J_\ell'(\eta)N_\ell'(\xi)} . \qquad (15)$$

Depending on the sign of the parameter ξ^2 in Equation (11), we can identify two branches of electromagnetic waves: The fast wave ($\xi^2 > 0$), characterized by the phase velocity $v_{ph} = \omega/k$ greater than speed of light ($v_{ph} > c$), and the slow wave ($\xi^2 < 0$).

In the helix-loaded waveguide there are two kinds of modes. There are the helix modes, and the hybrid fast wave modes composed of transverse electric (TE) and transverse magnetic (TM) modes. For a particular ξ and azimuthal mode number, ℓ, the helix mode is the lowest frequency mode. The helix mode is entirely supported by the helix and in general covers both the fast and slow-wave regions. In the limit where $R_c \to \infty$ it is the only mode that exists. Figure 4 shows the dispersion curves of the fast hybrid and helix modes.

If the dispersion curve is symmetric about the ω axis for a given frequency, the positive and negative wave numbers are the same. Equal amplitude waves traveling in the positive and negative axial direction can combine to form a pure sinusoidal standing wave. Standing waves can be produced by turning the waveguide into a cavity by covering the open ends with conducting plates. For a cavity Equation (2) becomes

$$\psi = \phi(r) \exp i(\ell\theta - \omega t) \frac{\sin kz}{\cos kz} .$$

The axial wave-number k is given by $n\pi/L$, where L is the length of the cavity and n is the axial mode number. The azimuthal and radial cavity mode patterns are the same as those of a waveguide; thus the cavity can be used to determine the waveguide dispersion characteristics.

Referring to Figure 4, the dispersion curves of the $\ell = 0$ modes are symmetric about the ω axis for both the helix and fast hybrid modes. When $\ell \neq 0$, the lower order fast hybrid modes are nearly symmetric about the ω axis. For these modes the cavity can be used to determine waveguide dispersion characteristics.

The dispersion curves of the helix modes for $\ell \neq 0$ are not symmetric about the ω axis. In this case the standing waves are not purely sinusoidal but an infinite sum of modes. This is because the boundry condition of zero tangential electric field at the end plate and the helix boundry condition of Equation (4) are not consistant. The azimuthal and radial cavity mode patterns are not the same in this case, thus for unsymmetrical modes the cavity cannot be used to measure waveguide dispersion characteristics.

SECTION 3

EXPERIMENTS

The purpose of the experiment is to verify the theoretical dispersion relation derived in Section 2 for the helix loaded cavity. The dispersion relation is an expression relating the frequency, ω, and the wave number, k. From this relation the phase velocity (v_p) and the group velocity (v_g) can be determined. The phase velocity equals ω/k and the group velocity equals $d\omega/dk$.

To experimentally determine the relation between ω and k those resonances belonging to the $\ell = 0$ helix mode, and the $\ell = 0$, $\ell = 1$, and $\ell = 2$ fast hybrid modes have to be identified, and the wavelength from which k can be determined has to be measured. Here ℓ is the azimuthal mode number.

To determine the wavelength of a given mode the distance between successive peaks of the field in the axial direction of propagation has to be measured.

To identify the modes, in addition to axial characteristics of the field mentioned above, the azimuthal and radial characteristics of the field have to be measured. It was shown in Section 2 that if the dispersion relation is symmetric in k, $[\omega(k) = \omega(-k)]$ for a given ω, then the azimuthal and radial field configuration will be unchanged by converting from waveguide to a cavity. The advantage of using a cavity over waveguide in measuring field configuration is that standing wave in a cavity is spatially static and therefore much easier to measure than the traveling wave in the waveguide.

Each cavity resonance will yield a standing wave mode that corresponds to one of the continuous waveguide modes. For a given waveguide mode the cavity has a resonant frequency at each value of the wave number, k, where k equals n π/L. Each resonance is a discrete point on the continuous waveguide dispersion curve.

A. EXPERIMENTAL APPARATUS

The experiment is centered around the helix loaded cavity. A photograph of the cavity with one of the end plates removed is shown in Figure 5. Figure 2 is a photograph of the helix. Figure 6 is a diagram of the cavity cross section. The cavity is a hollow aluminum cylinder with an inside radius, R_c = 3". Inside the aluminum cylinder is a concentric sheath helix made from Blue Macs flat cable #175-50. The helix construction is similar to that of a cardboard tube in a roll of paper towels. The two cavity parameters that affect the dispersion curves are the helix pitch angle, ϕ, and the ratio, R_h/R_c, of helix radius to cavity radius. Dispersion curves were measured for a pitch angle of 10° and R_h/R_c = .82 and .92.

The probe is a copper foil disk attached to a styrofoam wand. The wand is attached perpendicularly to a thin, 1/10" diameter, lucite rod. The rod lies along the axis of the cavity and exits both ends of the cavity through holes drilled in the end plates. With the rod the probe can be translated along or rotated about the axis of the cavity (see Figures 5 and 6).

Figure 7 is a photograph of the experimental apparatus and Figure 8 is a schematic of the apparatus. Microwave power is fed into the cavity by a sweep oscillator through an input coupler composed of a 1/8" diameter loop of wire that penetrates the cavity through one of the end plates. The output coupler is identical to the input coupler and enters the cavity through the opposite end plate. The couplers penetrate the end plates at a radial distance of 1.5

inches from the axis of the cylinder. The loops of the couplers lie in the
same plane and are connected together so that they rotate simultaneously.

The output coupler is fed into a spectrum analyzer. The output power at
a given input frequency to the cavity is proportional to the height of the
peak on the spectrum analyzer. The vertical output of the spectrum analyzer
is fed into the vertical input of a chart recorder. The lucite rod that
carries the probe is connected to the carriage of the chart recorder with
nylon thread. The other end of the lucite rod is attached to a counter weight
with nylon thread. Starting the internal linear horizontal drive of the chart
recorder pulls the probe through the cavity, and records the changes in the
field due to the perturbation of the probe.

B. MODE IDENTIFICATION METHOD

From a large number of possible resonances a particular family of
resonances belonging to the $\ell = 0$ helix and the $\ell = 0$, $\ell = 1$, and $\ell = 2$ fast
hybrid modes around which the theory was developed were identified. For
positive identification of these modes, it was sufficient to determine the
azimuthal and axial mode numbers. The radial mode numbers were not necessary
because the modes with the same axial and azimuthal mode number but different
radial mode number were sufficiently far apart in frequency not to be
confused.

The field configuration was identified by perturbing the cavity field
with a small metal probe and observing the change in output power caused by
the shift of the resonant frequency. Positions where the electric field is
maximum are perturbed the most and can therefore be located with respect to
zero electric field where perturbations are minimal. Variations in the

electric field in both the axial and azimuthal direction were measured. To measure the axial variation of the field a resonance is first located. This is accomplished by removing the effect of the probe by shorting it against an end plate. The sweep oscillator is tuned until a resonance peak is observed on the screen of the sprectrum analyzer; the probe is then pulled along the cavity axis by the chart recorder carriage. As the probe is moved it disturbs the field by causing a slight change in the resonant frequency of the cavity. Since the oscillator is initially tuned to the maximum of the resonance, a shift in cavity resonant frequency results in the oscillator being tuned to other than a maximum. This is seen on the spectrum analyzer as a change in the output power. Thus, the chart recorder records a negative of the field configuration; areas of maximum chart recorder amplitude are regions of minimum field strength and vise versa.

To measure the azimuthal variation of the field the lucite rod that carries the probe is detached from the chart recorder carriage. Keeping the axial position fixed, the probe is turned about the axis of the cylinder while the chart recorder carriage is moving, recording the azimuthal variation in the field.

Counting the number of nulls on the recorder image as the probe is pulled along or rotated about the cavity axis, determines the axial and radial mode number respectively. Figures 9, 10 and 11 are some examples of chart recorder outputs for fast hybrid modes.

Figure 12 shows how a too large probe could distort the field profile. Although the effect of a large probe was to distort the field profile, the azimuthal and axial symmetries on which mode identification was based were preserved. In fact some distortion enhanced the final picture by exaggerating the differences between regions of high and low field energy. To avoid too

much distortion it was found that the probe size should decrease with

increasing frequency to keep the probe size small compared to a wavelength.

To get a probe to have a measurable effect on the field was no problem

for the fast hybrid modes. A copper foil disk 1/4" to 1/2" in diameter was

sufficient. For the $\ell = 0$ helix mode to get a probe to have a noticeable

perturbation on the field required a large probe. It can be seen from Figure

13, a diagram showing the radial electric field for the $\ell = 0$ helix mode,

that the maximum field power is at the helix and decreases rapidly as one

moves away from the helix. For a probe to have a measurable perturbation on

the field the probe should be close to the helix and large enough to disturb a

significant portion of the field. To achieve this a 90° pie shaped wedge of

copper foil was used. The wedge was concentric with the cavity and its

circumference was nearly touching the helix.

At lower frequencies the resonant peaks of the helix modes were very low

amplitude even at maximum input power from the sweep oscillator. Some of the

peaks could barely be seen over the noise. To increase the amplitudes of

these modes, maximum coupling of the imput and output couplers with the field

was achieved by placing the couplers close to the helix where the field is a

maximum.

C. RESULTS

Mode density was the limiting factor in identifying modes at high

frequencies. It is well known that the number of cavity modes in a unit

frequency interval increases with the square of the frequency. Thus, at high

frequencies the modes overlap and their fields sum making mode identification

impossible.

The experiment produced 14 dispersion curves of fast hybrid modes plotted in Figure 14 thru 17. The curves are theoretical and the x's are the experimental results. The agreement between theory and experiment was good; within one percent for all data. From the data plots there are two fast hybrid modes for each value of ℓ. This is due to different radial mode numbers. There are an infinite number for each ℓ, but only the lowest 2 are accessable to the experiment due to mode crowding at higher frequencies.

The helix modes above $\ell = 0$ could not be measured in the resonant cavity experiment. Because of lack of symmetry about the $k = 0$ line, the helix modes with azimuthal symmetry greater than zero cannot form pure sinusoidal standing waves in the resonant cavity. Thus, the azimuthal and transverse wave number cannot be determined using the mode identification method mentioned above. The helix mode approaches a straight line when $R_h \rightarrow R_c$ and the dispersion equation is

$$\omega = \pm [kc\sin \phi + \ell (c/R_h) \cos \phi].$$

The slope can be varied by changing ϕ and the ω intercept by changing ℓ, R_h, and ϕ. The dispersion curve for the electron beam mode is a straight line in the (ω, k) parameter space. Thus, a wide band amplifier can be made by adjusting the slope and the ω intercept of the helix dispersion curve to overlap that of the electron beam mode.

As mentioned in Section 2 on theory, the dispersion curves of the helix for $\ell \neq 0$ are not symmetrical about the $k = 0$ line. In this case the standing waves are not pure sinsisoids, but the sums of modes needed to match both the end plate and helix boundary conditions. In this case the waveguide can not be described by cavity theory. Figure 18 shows an example of the axial variation of the field due to mode summing for a $\ell \neq 0$ helix mode.

CONCLUSION

This experiment investigated the properties of electromagnetic wave propagation in a helix loaded waveguide. The dispersion relations for the waveguide were obtained by examining the resonances of a cavity with the same radial cross section as the waveguide. From a large number of resonances those belonging to the $\ell = 0$ helix mode and the $\ell = 0$, $\ell = 1$, $\ell = 2$ fast hybrid modes were identified. The dispersion relation was obtained by plotting the resonant frequency against the axial cavity wavelength. (The helix modes with $\ell \neq 0$ could not be identified by the cavity experiment because of lack of symmetry about the $k = 0$ line.)

The agreement between theory and experiment for the identifiable modes was good. The largest deviation between theory and experiment was less than one percent.
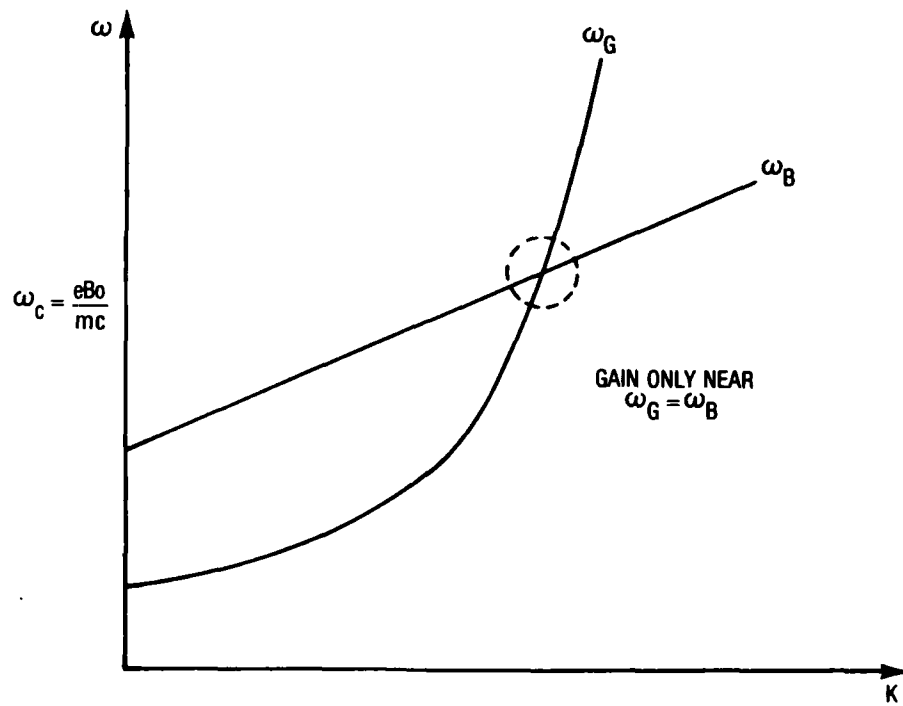
FIGURE 1. DISPERSION CURVES OF AN ELECTRON BEAM MODE AND A SLOW WAVE STRUCTURE MODE

FIGURE 2. SHEATH HELIX

HELIX

R_c

R_h

ϕ

CAVITY LENGTH = 6" R_c = 3"

R_h/R_c = .92 OR .82 ϕ = 10°
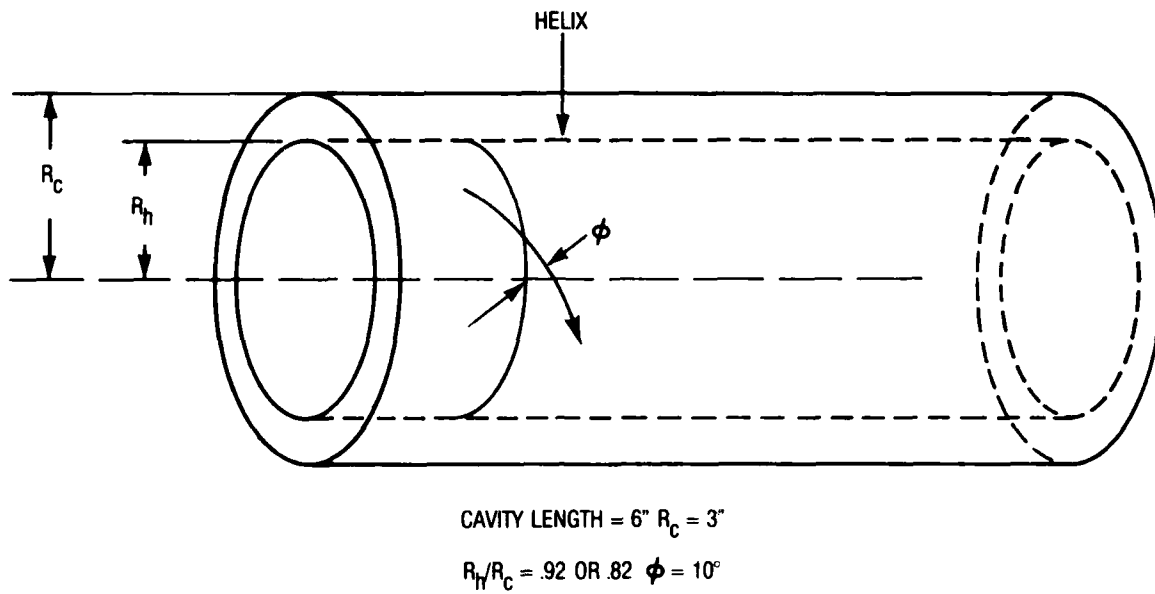
FIGURE 3. SHEATH HELIX LOADED WAVEGUIDE
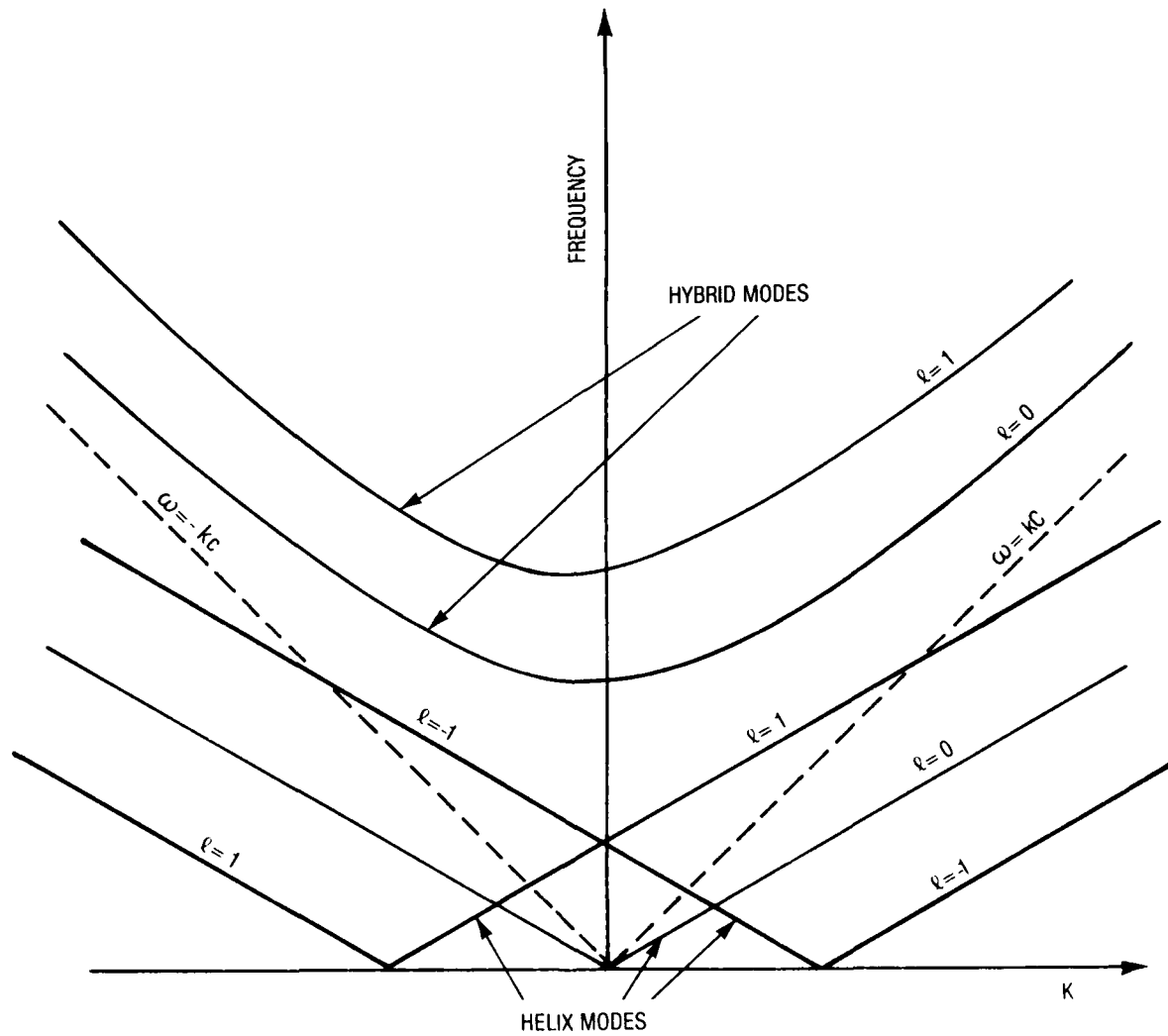
FIGURE 4. DISPERSION CURVES FOR HELIX LOADED WAVEGUIDE (NOTE ASYMMETRY OF HELIX MODES FOR $\ell \neq 0$)
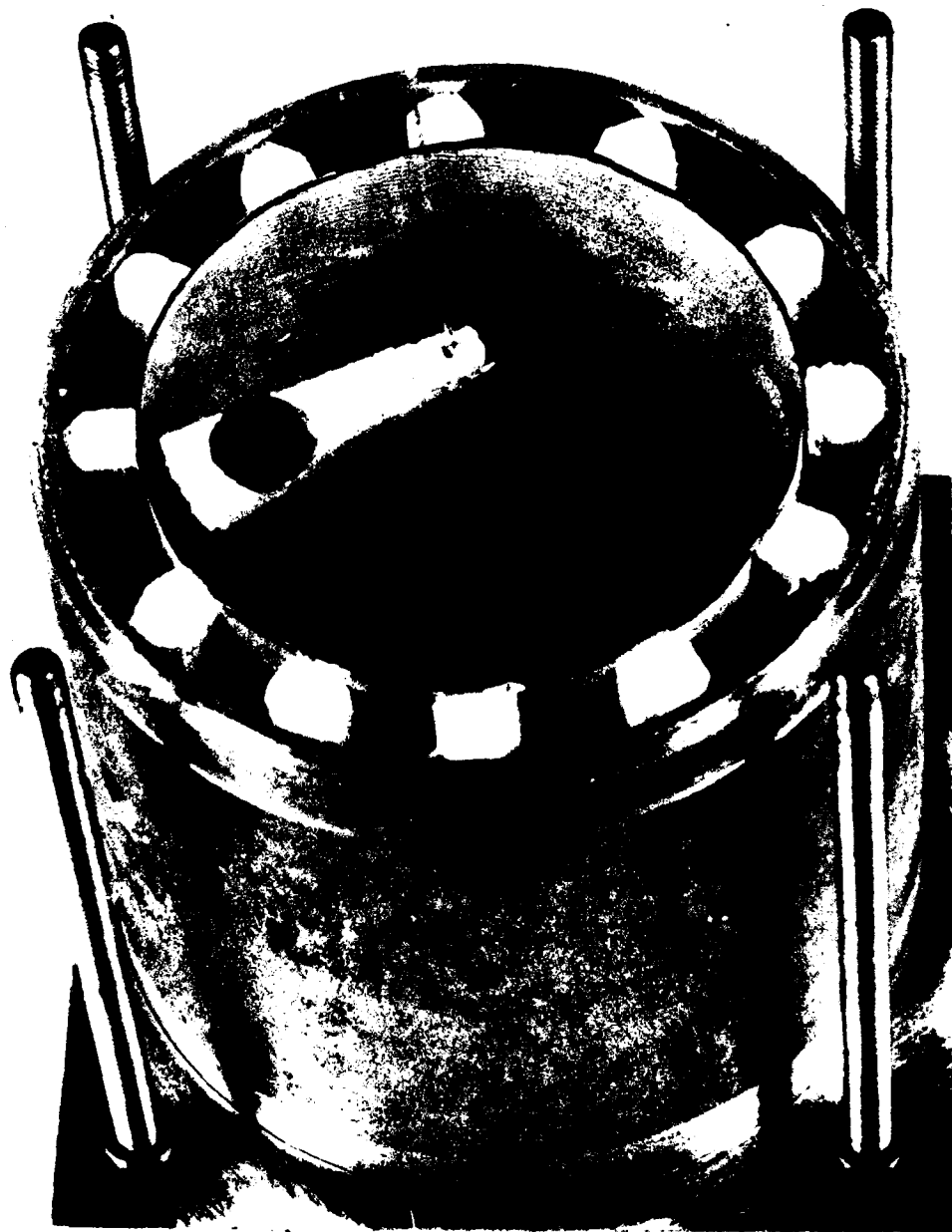
FIGURE 5. HELIX LOADED CAVITY
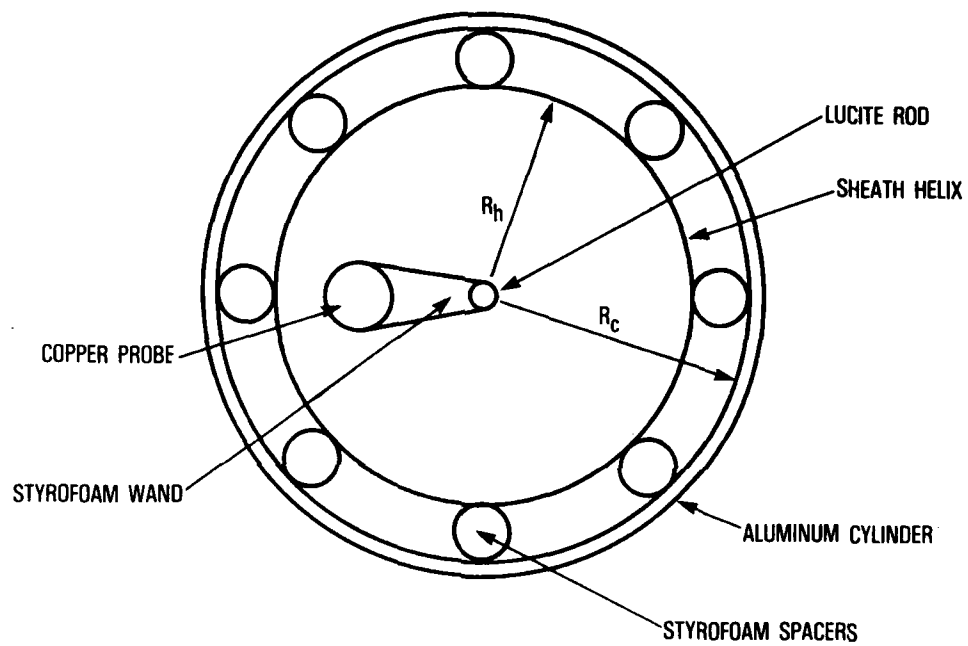
FIGURE 6. CROSS-SECTION OF HELIX LOADED CAVITY
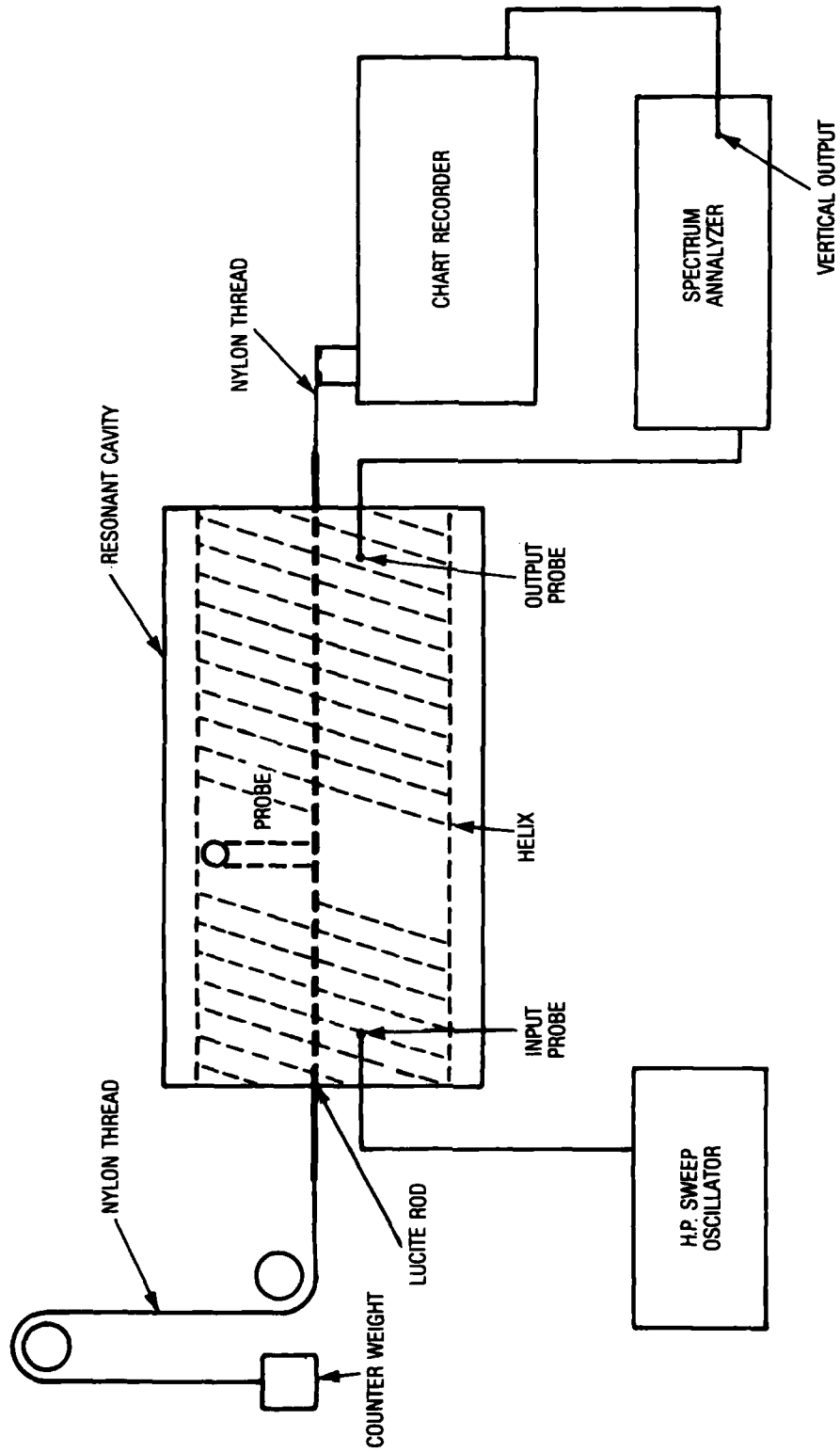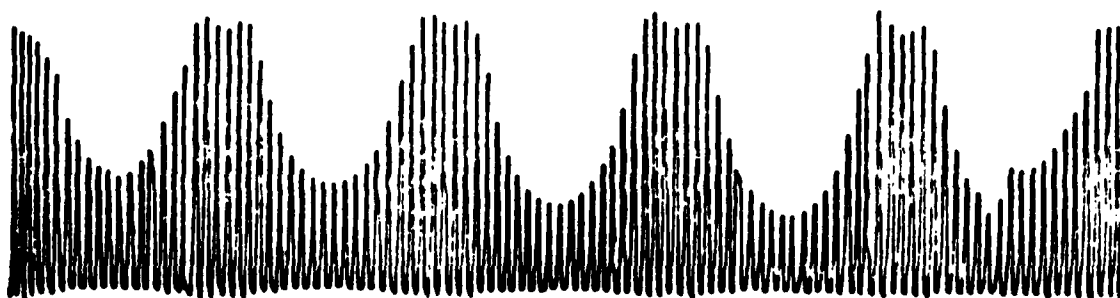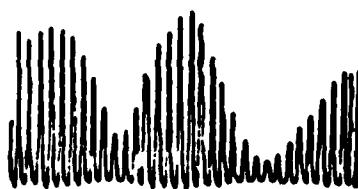
FIGURE 7. PHOTOGRAPH OF EXPERIMENTAL APPARATUS

FIGURE 8. DIAGRAM OF EXPERIMENTAL APPARATUS

AXIAL VARIATION

AZIMUTHAL VARIATION

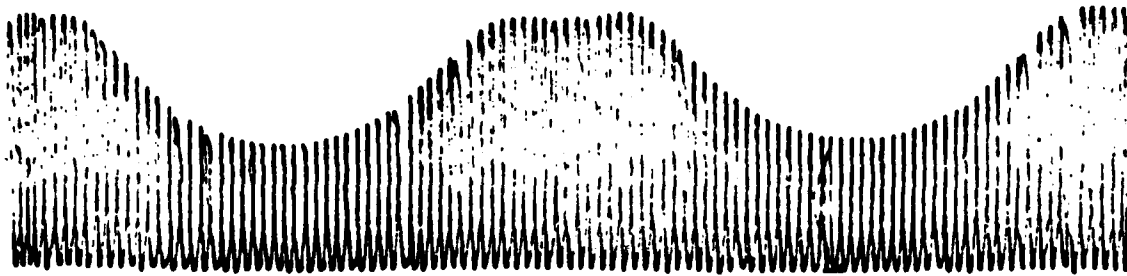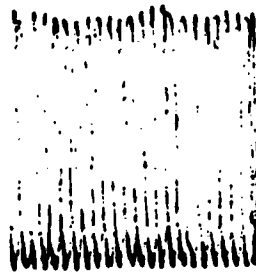FIGURE 9. FAST HYBRID MODE FREQ. = 5400MH$_z$, ℓ =1, n = 5, R_h/R_c = .82

AXIAL VARIATION

AZIMUTHAL VARIATION
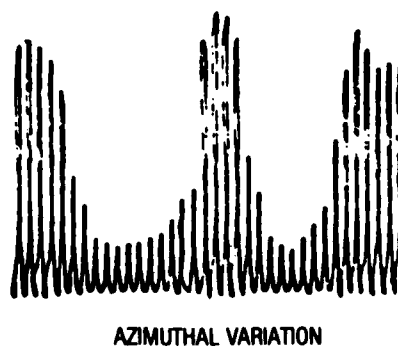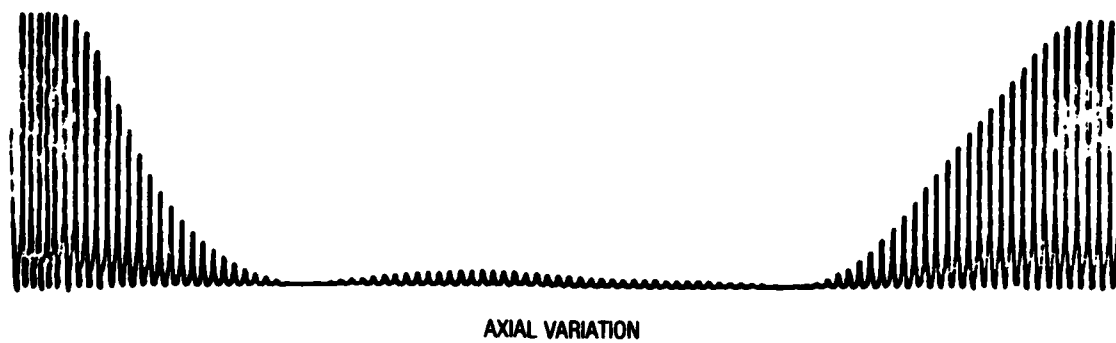
FIGURE 10. FAST HYBRID MODE FREQ. = 1689MH$_z$, ℓ = 1, n = 1, R$_h$/R$_c$ = .82

AXIAL VARIATION

AZIMUTHAL VARIATION

FIGURE 11. FAST HYBRID MODE FREQ. = 2455MH$_z$, ℓ = 0, n = 2, R$_h$/R$_c$ = .92
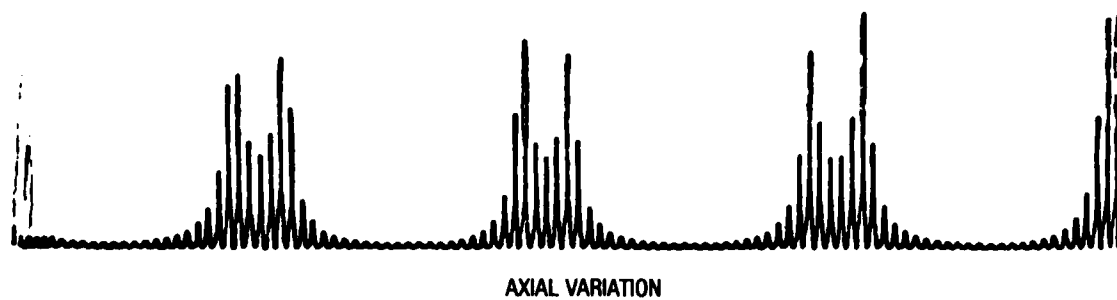
AXIAL VARIATION

FIGURE 12. AXIAL VARIATION OF FIELD SHOWING THE DISTORTION DUE TO TOO LARGE PROBE FREQ. = 4893 MH$_z$, ℓ = 1, n = 5
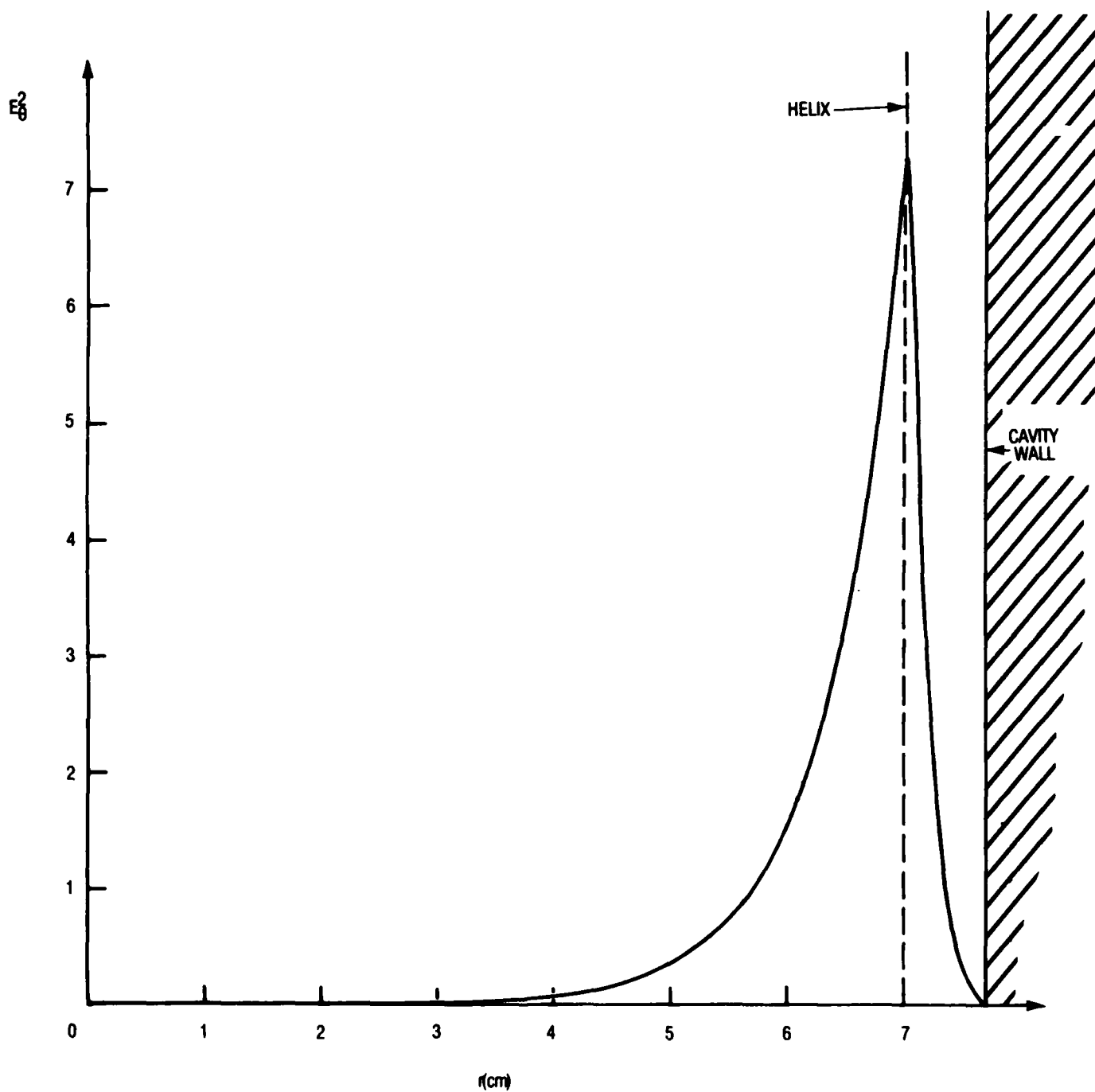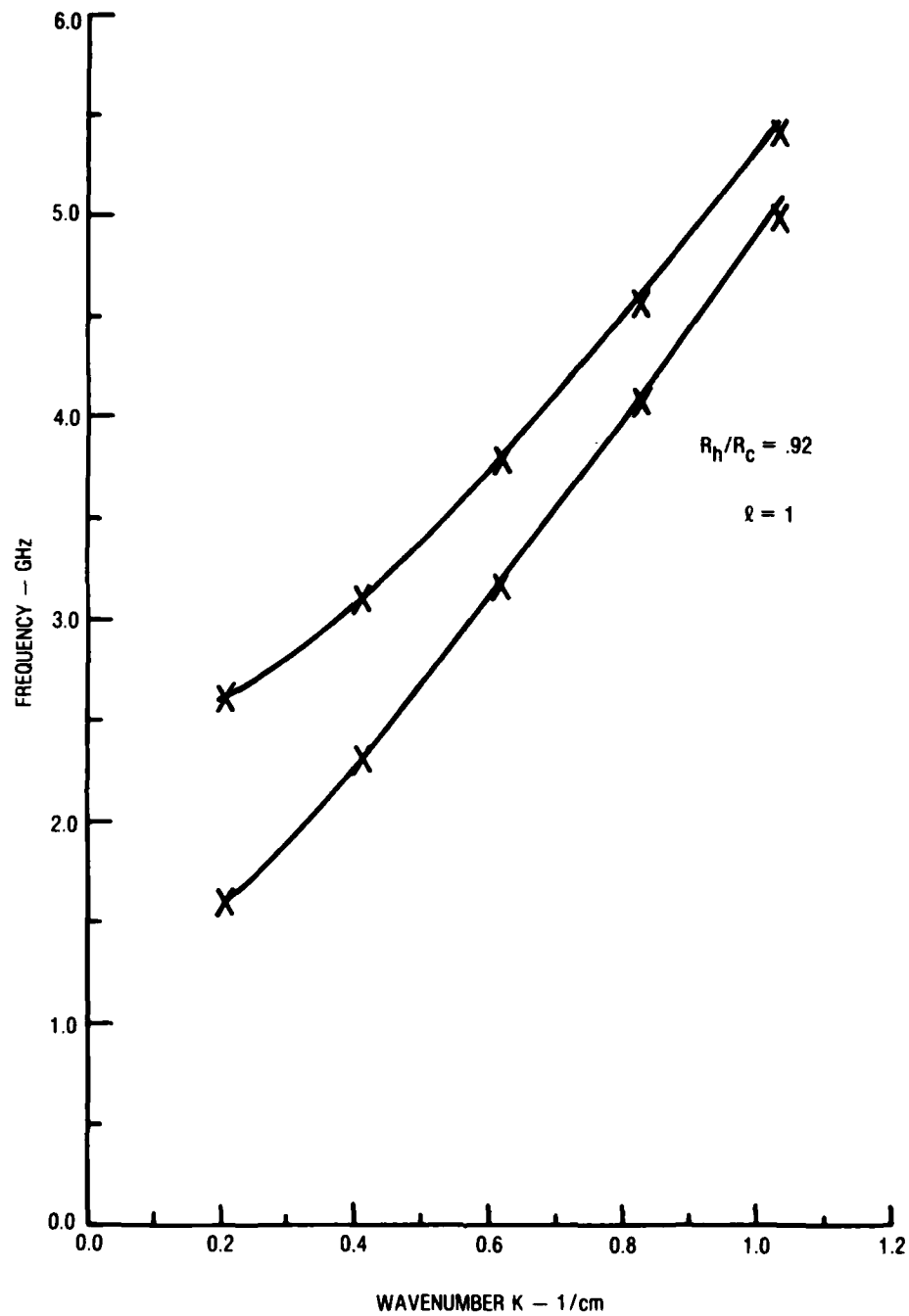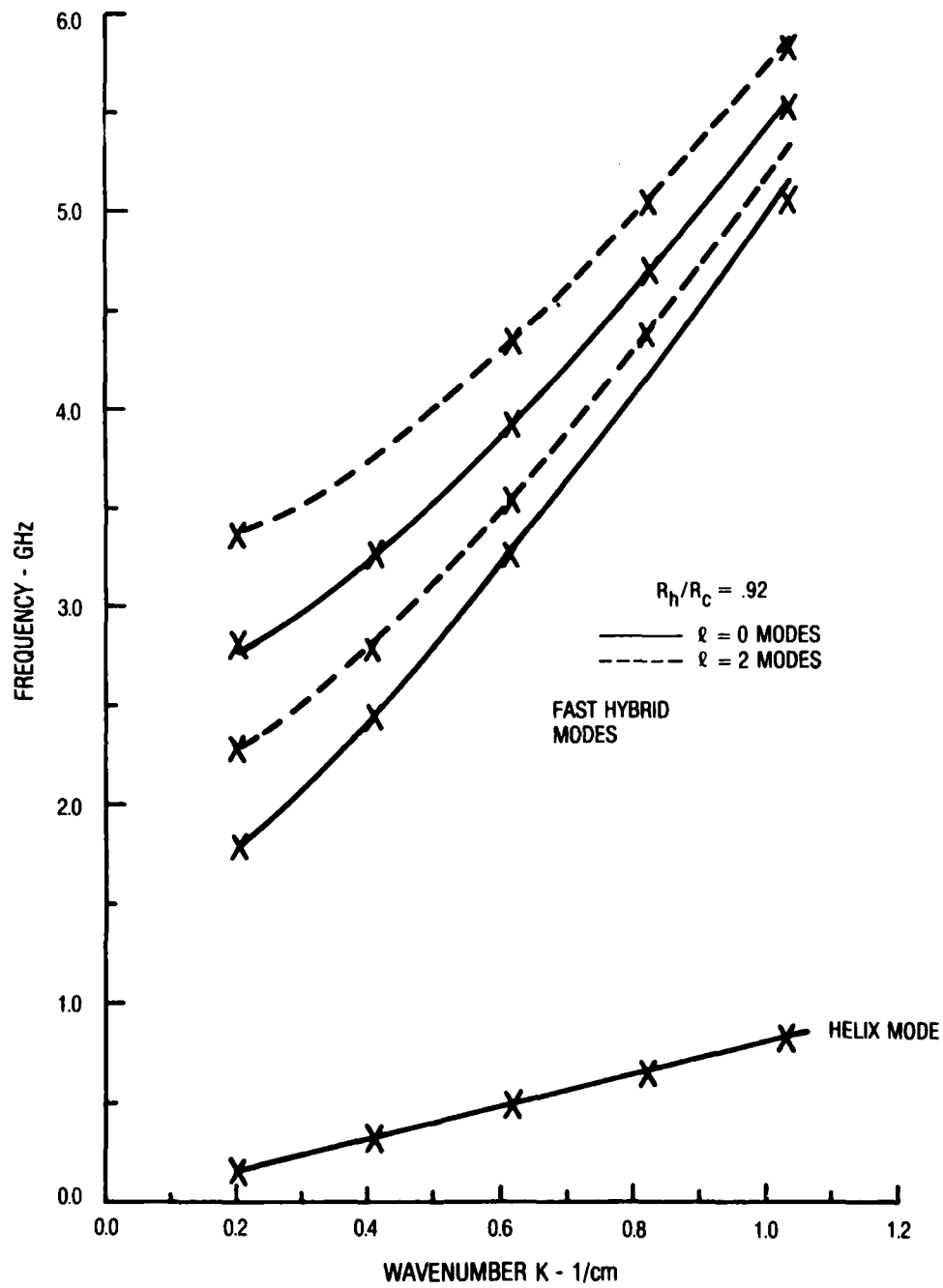
FIGURE 13. FIELD PROFILE OF HELIX MODE FREQ. $= 683.7 \text{MH}_z$, $\ell = 0$, n = 4, R_h/R_c = .92

FIGURE 14. DISPERSION CURVES FOR FAST HYBRID MODES $\ell = 1$, $R_h/R_c = .92$

FIGURE 15. DISPERSION CURVES FOR FAST HYBRID MODES. $\ell = 0$, $\ell = 2$, $R_h/R_c = .92$
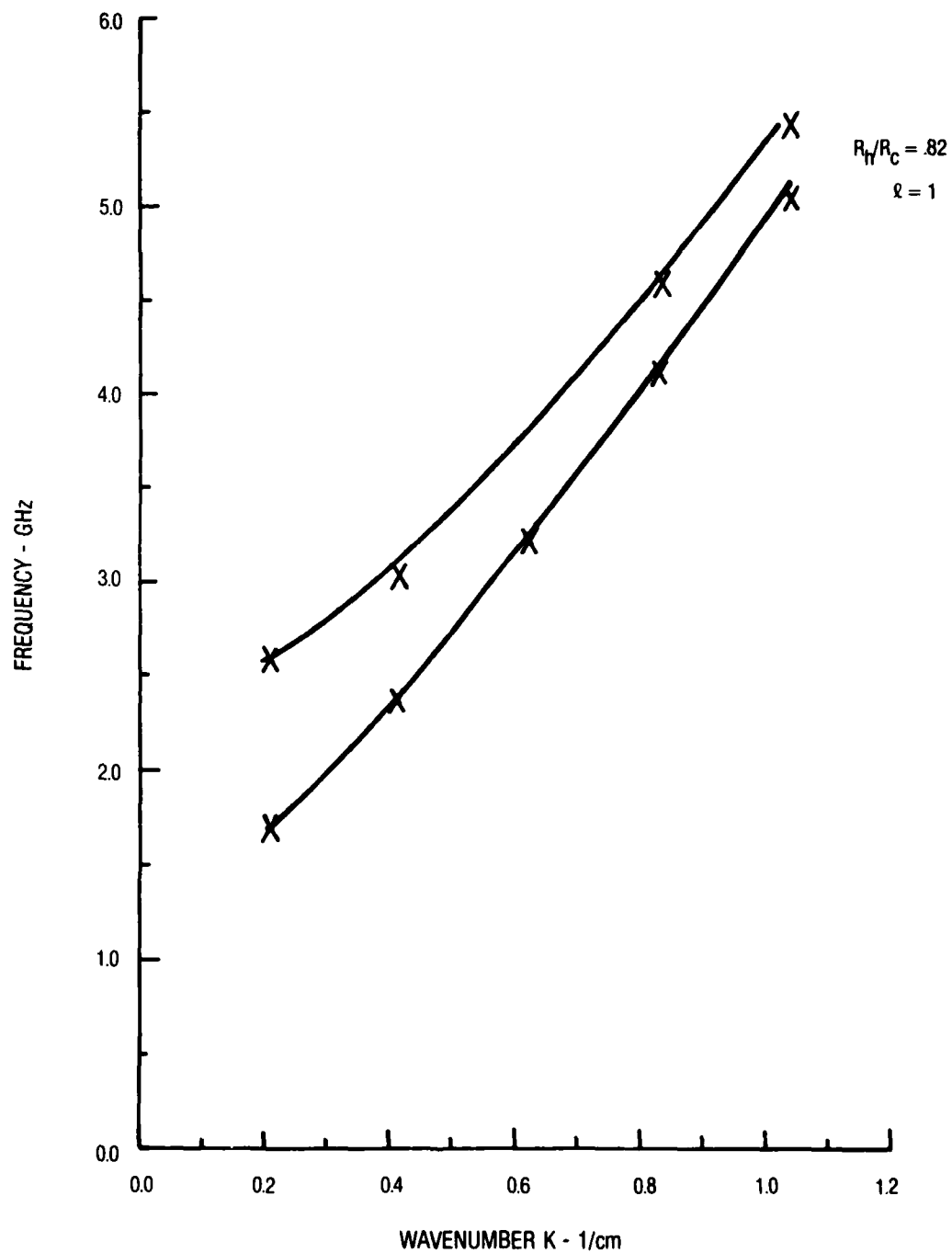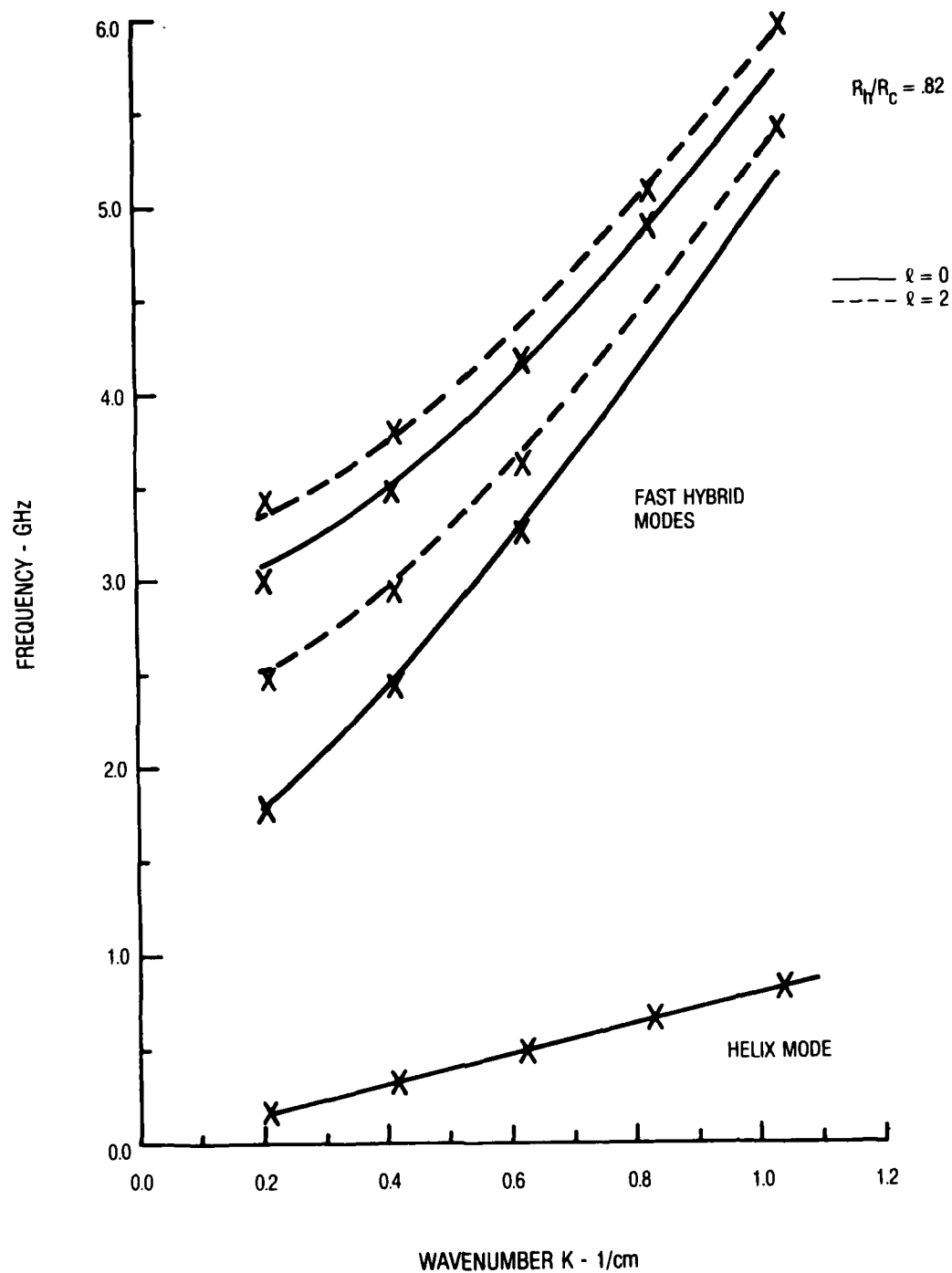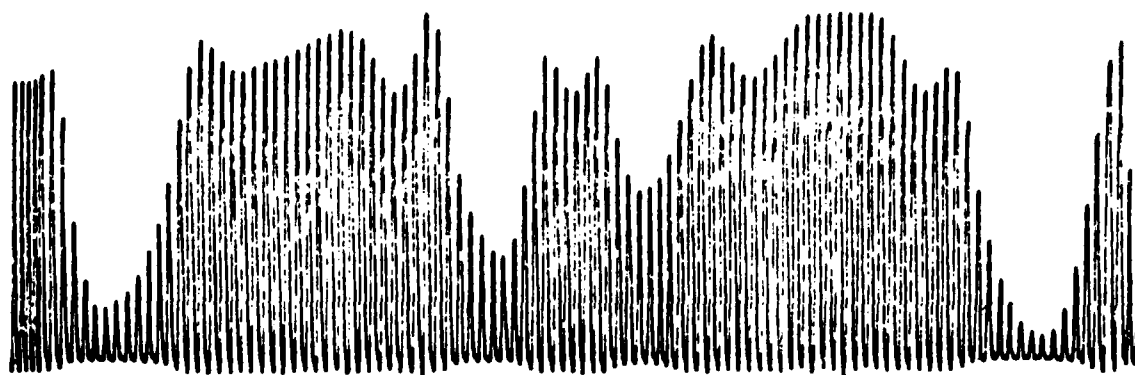
FIGURE 16. DISPERSION CURVES FOR FAST HYBRID MODES. $\ell = 1$, $R_h/R_c = .82$

FIGURE 17. DISPERSION CURVES FOR FAST HYBRID MODES $\ell = 0$, $\ell = 2$, $R_h/R_c = .82$

AXIAL VARIATION

FIGURE 18. AXIAL VARIATION OF HELIX MODE, $\ell = 0$, SHOWING EFFECT OF MODE
SUMMING FREQ. = 1084MHz, R_h/R_c = .82

REFERENCES

1. Choe, J. Y., and Uhm, H. S., "Theory of Gyrotron Amplifiers in a Disk or Helix Loaded Waveguide," Int. J. Electronics, Vol. 52, 1982, p. 729.

2. Uhm, H. S. and Choe, J. Y., "Properties of the Electromagnetic Wave Propagation on a Helix-Loaded Waveguide," J. Appl. Phys. Vol. 53, 1982, p. 8483.

DISTRIBUTION

	Copies		Copies

Chief
Office of Naval Research
Attn: Dr. C.W. Roberson   1
Arlington, VA 22217

Commander
Naval Research Laboratory
Attn: Code 6840 (Dr. S. Ahn)   1
     Code 6840 (Dr. A.K. Ganguly) 1
     Code 6840 (Dr. R. Parker)   1
     Code (Dr. Y.Y. Lau)   1
     Code (Dr. Pasour)   1
     Code (Dr. M.E. Read)   1
Washington, DC 20375

Defense Technical Information
 Center
Cameron Station
Alexandria, VA 22314   12

Library of Congress
Attn: Gift and Exchange Division 4
Washington, DC 20504

Harry Diamond Laboratory
Attn: Dr. H.E. Brandt   1
     Dr. A. Bromborsky   1
     Dr. A. Kehs   1
2800 Powder Mill Road
Adelphi, MD 20783

Lawrence Livermore National
 Laboratory
Attn: Dr. B. Kulke (L-436)   1
P.O. Box 808
Livermore, CA 94550

Massachusetts Institute
  of Technology
Attn: Prof. G. Bekefi   1
Bldg. 36-213
77 Massachusetts Ave.
Cambridge, MA 02139

Massachusetts Institute
  of Technology
Plasma Fusion Center
Attn: Dr. R. Temkin   1
Cambridge, MA 02139

Polytechnic Institute
  of New York
Attn: Dr. S.P. Kuo   1
Route 110
Farmingdale, NY 11735

University of Maryland
Electrical Engineering Dept.
Attn: Prof. W. Destler   1
     Prof. V.L. Granatstein 1
     Prof. C.D. Striffler   1
     Dr. W. Lawson   1
College Park, MD 20742

University of Maryland
Plasma Physics Laboratory
Attn: Dr. W.M. Chang   1
College Park, MD 20742

University of Maryland
LPFE
Attn: Dr. Guillory   1
College Park, MD 20742

(1)

DISTRIBUTION

	Copies		Copies
University California Los Angeles Department of Electrical Engineering Attn: Dr. D.B. McDermott Los Angeles, CA 90024	1	Raytheon Company Attn: Dr. T. Ruden Code C52-58 Bedford, MA 01730	1
Yale University Mason Laboratory Attn: Prof. J.L. Hershfield 400 Temple St. New Haven, CT 06520	1	Internal Distribution: E231 E232 R41 (J. Smith) R41 (H. Uhm) R43 (J. Cunningham)	9 3 1 1 1
Dartmouth College Department of Physics Attn: Dr. J.E. Walsh Hanover, NH 03755	1	R43 (J. Choe) R43 (H. Crosby) R43 (D. Jablonski) R43 (A. Krall) R43 (W. Namkung)	1 10 1 1 1
Mission Research Corporation Attn: Dr. D. Sullivan 1730 Randolph Rd., SE Albuquerque, NM 87106	1		
Pulse Science Attn: Dr. G. Proulx 14796 Wicks Blvd. San Leandro, Ca 94577	1		
Science Applications, Inc. Attn: C.L. Chang 1710 Goodridge Dr. McLean, VA 22102	1		
Varian Associates Attn: Dr. H. Jory Bldg. 1 611 Hansen Way Palo Alto, CA 94303	1		
Raytheon Company Attn: Dr. A. Palevsky Dept. 3671, Code 47 Waltham, MA 02116	1		

(2)

END

DTIC

5-86